ACS OMEGA

http://pubs.acs.org/journal/acsodf

Article

Integrated Micropillar Polydimethylsiloxane Accurate CRISPR Detection System for Viral DNA Sensing

Kenneth N. Hass, Mengdi Bao, Qian He, Li Liu, Jiacheng He, Myeongkee Park, Peiwu Qin, and Ke Du*

Cite This: *ACS Omega* 2020, 5, 27433−27441

Read Online

ACCESS | Metrics & More | Article Recommendations | Supporting Information

ABSTRACT: A fully Integrated Micropillar Polydimethylsiloxane Accurate CRISPR deTection (IMPACT) system is developed for viral DNA detection. This powerful system is patterned with high-aspect-ratio micropillars to enhance reporter probe binding. After surface modification and probe immobilization, the CRISPR-Cas12a/crRNA complex is injected into the fully enclosed microchannel. With the presence of a double-stranded DNA target, the CRISPR enzyme is activated and denatures the single-stranded DNA reporters from the micropillars. This collateral cleavage releases fluorescence reporters into the assay, and the intensity is linearly proportional to the target DNA concentration ranging from 0.1 to 10 nM. Importantly, this system does not rely on the traditional dye-quencher-labeled probe, thus reducing the fluorescence background presented in the assay. Furthermore, our one-step detection protocol is performed on-chip at isothermal conditions (37 °C) without using complicated and time-consuming off-chip probe hybridization and denaturation. This miniaturized and fully packed IMPACT chip demonstrates sensitive and accurate DNA detection within 120 min and paves ways to the next-generation point-of-care diagnostics, responding to emerging and deadly pathogen outbreaks.

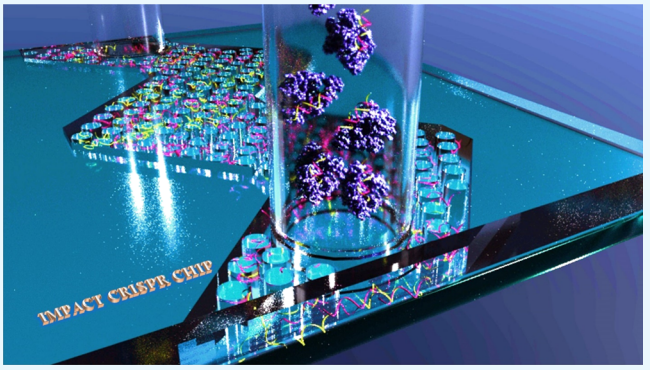

INTRODUCTION

The widespread impact of the current coronavirus disease (COVID-19) is a striking indicator of the fact that the global community is struggling to battle infectious diseases. Failure to contain the virus early has resulted in an outbreak that has infected over 36.5 million people and led to over 1 million deaths.[1,2] The current situation highlights an urgent need for access to real-time detection that is accurate and effective to identify those infected, so they can be properly quarantined and treated.[3,4] An effective vaccine could be the best solution to contain epidemics. However, vaccines take a very long time to be developed, as evidenced with the African swine fever virus (ASFV), which was initially discovered in 2018, but only in January of this year was the preliminary vaccine announced.[5] It took over an additional month to demonstrate its effectiveness in laboratory tests, and it still needs to be proven effective in the field.[6]

Currently, there are no proven treatments for either SARS-COV-2 (severe acute respiratory syndrome coronavirus 2) or ASFV. Even if one would to be developed soon, it can take years to prove its effectiveness in clinical trials and for mass production of the vaccine, needless to mention its distribution and administration in affected areas.[7] To contain and prevent the spread of these contagious outbreaks, a rapid point-of-care (POC) testing device is essential. Current methods can take up to 2 days for tittering in a centralized laboratory in order to diagnose whether a sample contains the disease and are not viable or efficient when trying to isolate those infected and prevent them from spreading the disease to others.[8,9]

In addition, the collected patient samples need to be sent to a centralized laboratory, leading to very long turnaround times and greatly limiting the number of people who could be tested and confirmed.[10] Strides have been made to develop POC detection methods which can be deployed in the field, and currently lab-on-chip (LOC) devices or simple test kits which involve real-time polymerase chain reaction (RT-PCR) have emerged as one of the leading choices for meeting the desired criteria.[11] RT-PCR is particularly sought after due to its ability to amplify the viral RNA/DNA from a few copies to billions.[12] It has also been shown to work with clinical samples in LOC devices with low volumes of both reagents and patient samples.[13] However, there have been many issues with implementing PCR test kits, such as shortages in test kits

Received: August 13, 2020
Accepted: September 30, 2020
Published: October 13, 2020

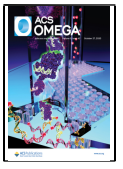

https://dx.doi.org/10.1021/acsomega.0c03917
ACS Omega 2020, 5, 27433−27441

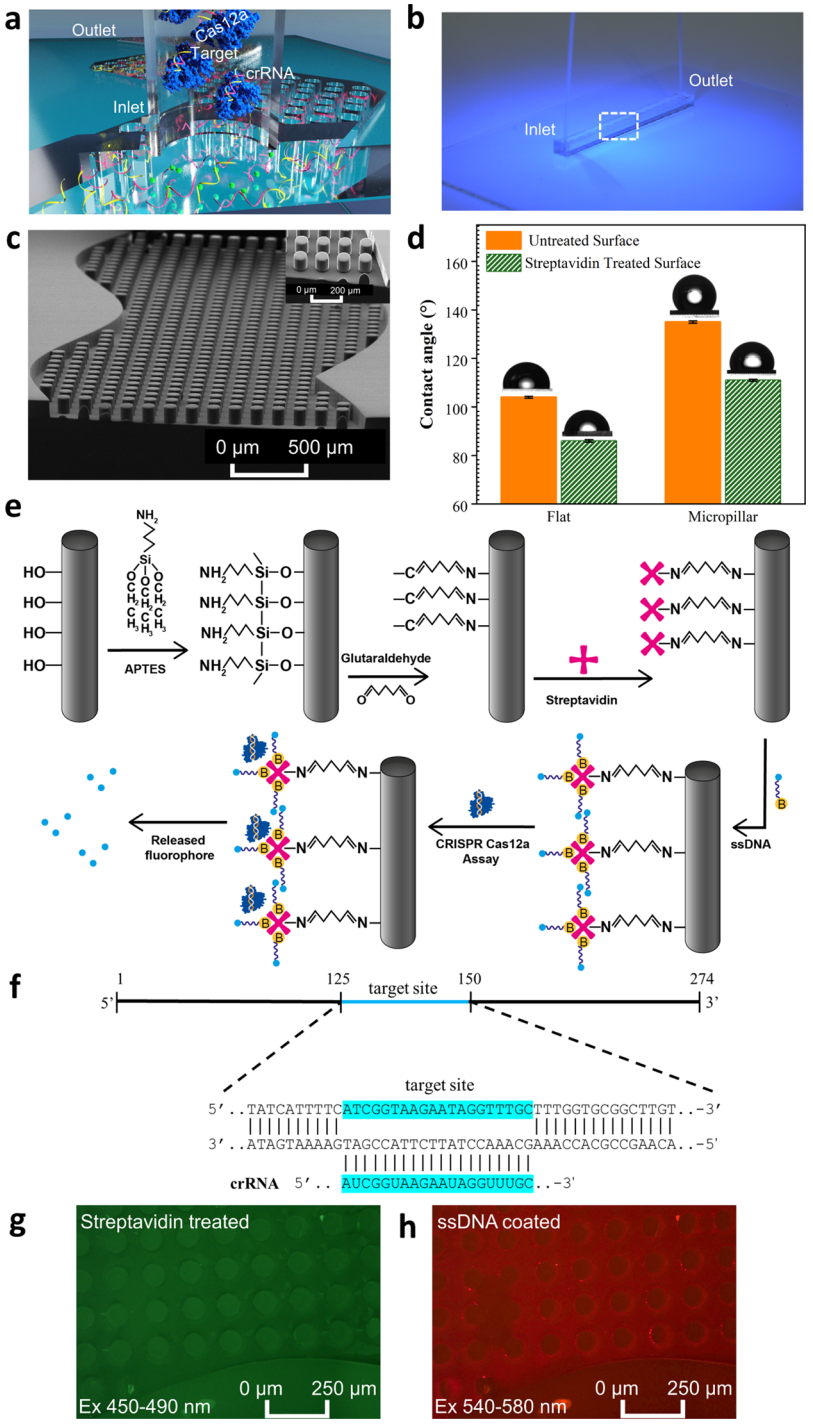

Figure 1. (a) Schematic of the clustered regularly interspaced short palindromic repeats (CRISPR)-based IMPACT chip DNA detection. (b) Photograph of the IMPACT chip. The dashed white box indicates regions patterned with micropillars. (c) SEM image of the micropillars. Inset: high magnification image. (d) Static water contact angle measurement on both flat and micropillar surfaces before (orange) and after (green) surface treatment. (e) Schematic of the surface treatment protocol, ssDNA probe binding, and CRISPR detection. (f) ASFV target DNA sequence and the corresponding crRNA sequence. (g) Fluorescent image of the channel which received chemical treatment and streptavidin binding (green fluorescence). (h) Fluorescent ssDNA-covered IMPACT chip, showing red fluorescence.

and trained professional to use them, as well as potential inaccurate results from the kits.[14,15]

CRISPR provides an alternative to PCR amplification techniques for the detection of viral RNA/DNA. Certain Cas proteins, such as CRISPR-Cas12a, have been shown to be powerful in biological detection due to their ability to indiscriminately cut single-stranded DNA (ssDNA) after they are activated by a target DNA.[16] This is extremely useful when they are paired with "reporter probes" (ssDNA strands with a fluorescent dye and quencher attached to them), as the CRISPR complex can cleave the reporter probe and release the dye for fluorescence quantification. CRISPR-Cas12a has also shown the ability to distinguish a single base pair mismatch in the target.[17,18] However, one of the issues with utilizing the

https://dx.doi.org/10.1021/acsomega.0c03917
ACS Omega 2020, 5, 27433−27441

CRISPR complex is the high fluorescence background signal associated with the sample as the quencher cannot fully quench the fluorescent dye.

Solid-phase detection assays have been developed as one potential solution to overcome this issue presented in the liquid phase. On the solid surface, reporter probes do not require a quencher since they are only measured in the liquid phase after degradation; thus, the fluorescent signal will be largely reduced without the target DNA present in the assay. However, an extended surface with a larger surface area is always needed to increase the probe binding capacity. It has been shown that these extended surfaces can increase the amount of probe binding, lower the detection limit of the target of interest, and extend the detection dynamic range.[19,20]

Here, we present a fully enclosed Integrated Micropillar Polydimethylsiloxane Accurate CRISPR deTection (IMPACT) system for nucleic acid target detection on the solid-surface of polydimethylsiloxane (PDMS) utilizing CRISPR-Cas12a. The reporter probes were first immobilized in the enclosed microchannel, and the CRISPR complex was pumped into the system for reaction (Figure 1a). Leveraging the high activity of CRISPR-Cas12a enzyme and the ability of micropillars to bind more reporter probes, we successfully detected a double-stranded DNA target without background issues. In addition, the IMPACT chip requires low volumes of reagents, operates in a one-step detection fashion, and does not require complicated temperature control, making it ideal for POC applications. To prove the concept of the IMPACT chip for viral DNA detection, the target sequence selected for the crRNA was synthesized after a segment of the ASFVSY18 genome (B646L). This sequence has been shown in past works to work well with CRISPR-Cas12a and has a high selectivity when exposed to mismatches between the crRNA and target DNA.[21,22] In the future, by integrating CRISPR-Cas13a, our device could also work with RNA-based pathogens, such as the emerging SARS-COV-2.[23,24]

RESULTS

The IMPACT chip (Figure 1b) consists of 6 cm long channels patterned with PDMS micropillars. The PDMS micropillars were perpendicular to the bottom of the channel, and the spacing between the micropillars was 50 μm. Every SU-8 channel mold contained 4941 microholes from which PDMS micropillars could be formed. For experiments utilizing a flat channel, the channel dimensions and depth were the same, except that there were no micropillars within the channel. Figure 1c shows the scanning electron microscopy (SEM) image of the channel, revealing the periodic curved nature of the channel and even spacing of the micropillars (diameter: 100 μm; height: 120 μm). After channel fabrication and sealing, surface treatment with APTES (3-aminopropyl)-triethoxysilane and glutaraldehyde (GA) was performed for streptavidin immobilization.[25] After streptavidin coating, the static water contact angle decreases from ∼105 to ∼90° for a flat PDMS surface and ∼138−110° for micropillar surface, respectively (Figure 1d). The addition of streptavidin makes the surface more hydrophilic as the surface becomes more polar compared to PDMS, but overall, the contact angles remain high due to the neutral (non-polar) nature of streptavidin.[26] Figure 1e shows the entire sample preparation and detection protocol. DNA reporter probes with a biotin label were conjugated on the streptavidin-coated micropillars. The CRISPR-Cas12a complex was then introduced into the channel. With the presence of the ASFV target DNA, it cleaves the reporters from the micropillars for detection. The sequences of the DNA target and the crRNA are listed in Figure 1f. The target was selected based on the PAM region in the ASFV-SY18 genome.[21] It has been shown that auto-fluorescence occurs from the chemical treatment of APTES and GA.[27] In our case, we were able to confirm that the phenomenon was specific to GA and APTES (Figure S1a) and use it to show that it only occurs on PDMS in the presence of these chemicals (Figure S1b). Figure 1g shows the uniformity of the chemical treatment on the surface, as the intensity of the auto-fluorescence (emission: 525 nm) is uniform throughout. We then incubated the reporter probes (Cy-5 dye, emission: 668 nm) in the channel for 3 h and showed uniform coating in the channel (Figure 1h).

After establishing a surface modification and streptavidin incubation strategy, we first determined the channel washing conditions. After incubating biotinylated photocleavable reporter probes (/5PCBio/TTATTCTTATTGTGT-GAACTGCTCCTTC TTGACTCCACC/36-FAM/) in the channel for 3 h, the channel was washed with 75 μL DI water. The photocleavable linker is a function group added in the probe sequence and can be dissolved by ultraviolet (UV) exposure. Then, the channel was evacuated, and the fluorescence intensity of the supernatant was immediately evaluated. After the first wash, a high fluorescence peak was observed for all the samples (Figure 2a), indicating that excessive DNA probes were washed from the channel. During this step, the additional binding capacity provided by the streptavidin treatment and extended surface is first seen. Both the treated micropillar and flat channel have lower signals compared to the untreated channel, meaning fewer excess probes were washed from the treated channels. Furthermore, comparing the treated flat and micropillar channel, the micropillar channel has a lower signal, meaning the extended surface also increased binding capacity, leading to less probes being flushed out. A second wash was performed to confirm that the unbounded DNA probes were completely removed from the channel.

After the second wash, the collected supernatant barely shows any fluorescence peak. As shown in Figure 2b, the integrated signal (490−700 nm) for the first supernatant ranges between ∼8000 and 9000 counts, regardless of surface treatment conditions, as the spectrometer signal was saturated due to the high amounts of the washed out reporter probes. On the other hand, the integrated signal for the second supernatant is only ∼300 counts, eliminating the background caused by weakly bounded DNA probes. After washing, the bounded reporter probe was released by UV exposure, and the results are presented in Figure 2c. The flat channel coated with streptavidin shows ∼3 fold more reporter probe binding than the uncoated surface. In addition, the micropillar channel coated with streptavidin shows the highest signal among the three substrates.

With an optimal washing condition in hand, we then studied the effect of incubation time for biotin-labeled DNA binding on the streptavidin-coated PDMS surface. After channel surface modification and streptavidin treatment, fluorescent reporter probes were introduced to bind on the solid surface. Then, the washing protocol was performed, followed by UV light exposure to retrieve the reporter probe. As shown in Figure 3, for the streptavidin-coated surface, the number of DNA immobilized on the surface does not show a significant

https://dx.doi.org/10.1021/acsomega.0c03917
ACS Omega 2020, 5, 27433−27441

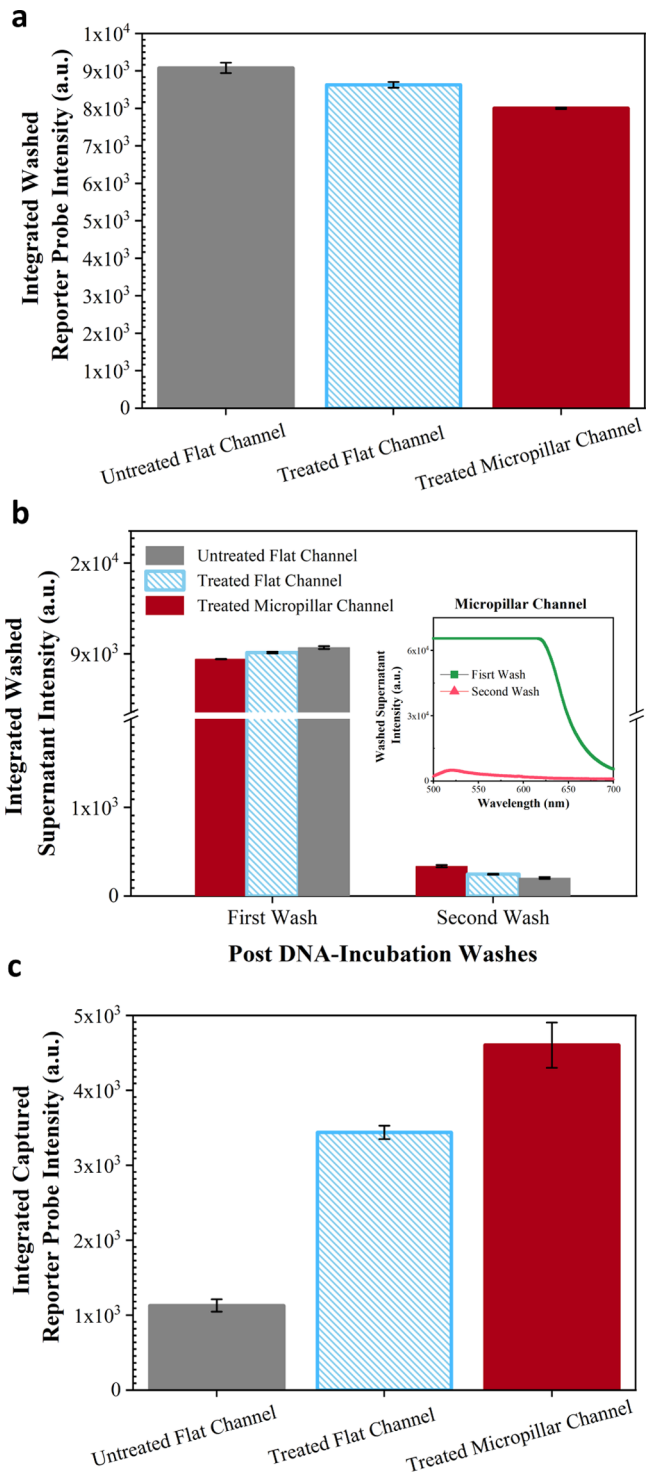

Figure 2. Washing data for flat and micropillar channels. The treated flat and microchannel samples were coated with streptavidin. (a) Integrated intensity of supernatant after first wash with 75 μL of DI water through channel. (b) Comparison of integrated intensity of the supernatant after washing 75 μL of DI water through the channel the first and second time. Inset shows the uncorrected emission curve of washed reporter probe for the treated micropillar channel. (c) Integrated intensity of reporter probes released with UV light exposure. Error bars are standard deviation of the mean.

change with an incubation time between 10 and 60 min as the integrated fluorescence intensity of the retrieved DNA ranges between 4500 and 5500 counts. However, the binding capacity

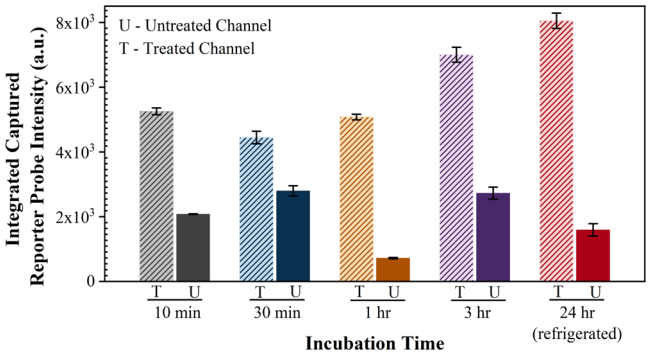

Figure 3. Released reporter probe intensity versus incubation time (10 min to 24 h). Treated samples received surface modification and streptavidin treatment before photocleavable reporter probe incubation (1 nmol). The sample was retrieved via UV photocleavage. Error bars are standard deviation of the mean.

increases ~25% with 3 h incubation when compared to 10 min incubation. Although the binding capacity further increases with 24 h incubation, it requires refrigeration as the streptavidin protein could denature at room temperature. On the other hand, the negative sample without streptavidin coating does not show a correlation to the incubation time, indicating less specific binding. Moreover, the negative sample always shows much lower fluorescence intensity than the positive sample. For example, with 3 h incubation, the retrieved DNA from the positive sample is ~2.6 times higher than that from the negative sample. It further indicates that surface modification can enhance the probe binding capacity. Therefore, we used 3 h incubation to prepare the IMPACT chip for solid phase CRISPR detection.

The extended surface provided by high-aspect ratio micropillars significantly increases the reporter probe binding capacity. To demonstrate this, we compared the number of captured DNA molecules on the micropillar channel with that of the flat channel (Figure 4). With an input of 0.01 nmol, the retrieved DNA from the micropillar channel has an integrated intensity of ~2000 counts, which is much higher than that of the flat surface (~900 counts). With an input of 0.1 nmol, the retrieved DNA from the micropillar channel has an integrated intensity of ~5500 counts and is ~40% higher than that of the

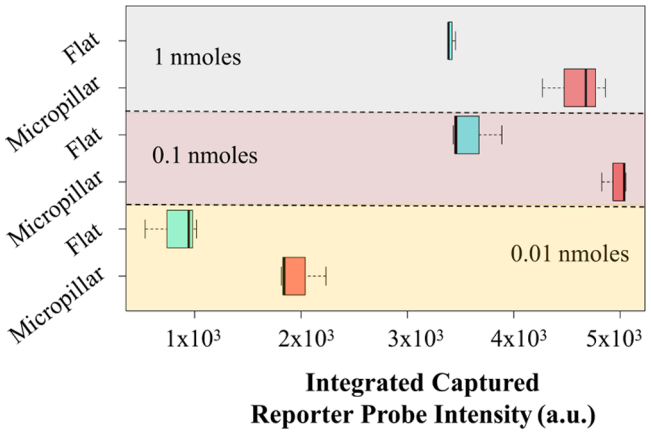

Figure 4. Released ssDNA reporter probe integrated intensity for flat and micropillar channels with a DNA input load of 1, 0.1, and 0.01 nmol. UV photocleavage was used to retrieve the ssDNA reporter probes. The skewness of each dataset is presented by boxplot.

https://dx.doi.org/10.1021/acsomega.0c03917
ACS Omega 2020, 5, 27433−27441

flat channel. With an input of 1 nmol, the micropillar channel still shows a higher signal than the flat channel but is comparable to 0.1 nmol sample, indicating that the channel is saturated with an input of ~0.1 nmol. Thus, we used 0.1 nmol reporter probes in our CRISPR detection as higher load could cause unnecessary background.

We combined the DNA probe modified micropillar channel with CRISPR-Cas12a assay for solid-phase and background free viral DNA sensing. We first mixed CRISPR-Cas12a/crRNA/target DNA in an Eppendorf tube and then injected the complex into the IMPACT chip and allowed it to incubate for 2 h. Figure S2 shows more data on optimal CRISPR incubation time in the liquid phase, and 2 h was chosen due to the large increase in the signal compared to 1 h, compared to the relatively small increase between 2 and 3 h. The activated complex diffuses in the microchannel and nonspecifically cleaves the reporter probes from the micropillars. The uncorrected emission curve and the integrated fluorescence signal of the CRISPR experiments are shown in Figure 5a and 5b, respectively. The measured fluorescence intensity linearly increases with the target concentration ranging from 0.1 to 10 nM (Pearson's R = 0.9778). On the other hand, the supernatant without any ASFV target DNA input does not present a fluorescence signal as the CRISPR-Cas12a cannot be activated, demonstrating a fully enclosed and efficient micro-device for ultra-low background viral DNA quantification.

DISCUSSION

We have shown that the PDMS micropillars provide a significant increase in solid-state reporter probe binding compared to the flat surface. The increased ssDNA reporter probe capacity can extend the detection limit and also the dynamic range.[28,29] In addition, the micropillar array increases the interaction between biomolecules and the substrate, as the surface area in contact with any given solution is significantly higher. To further increase the probe binding capacity, we can increase the aspect ratio of PDMS micropillars and the microchannel length. Indeed, the channel was designed to have a periodic curvature throughout its length in order to show its ability to utilize a curved design with the chip, which in the future could snake back and forth across an entire sample, greatly increasingly the overall surface area. The aspect ratio of the microstructures can be further increased by choosing more rigid materials. For example, an aspect ratio of 160:1 has been demonstrated on silicon by using deep-ion reactive etching.[30,31] Silicon would also have the advantage of potentially removing some of the air bubbles seen during use with the IMPACT chip, which could ensure greater uniformity in coating of reporter probes. Alternatively, the emerging additive manufacturing technology can also be used to create such ultra-high aspect ratio microstructures as an efficient target capture platform.[32,33]

One of the main advantages of the IMPACT chip compared to traditional CRISPR assays is its ability to limit the background caused by dye-quencher probes, which is typically seen in CRISPR detection in the liquid state and needs to be designed around to lower the detection limit.[34,35] Our device utilizing solid-phase CRISPR does not need to tether a quencher on the probe. The cleaved CRISPR products are sent to a separate reservoir for detection, thus completely avoiding the fluorescence background caused by the tradition "one pot" detection. As shown in Figure 5, without the presence of ASFV target DNA, virtually no fluorescence background signal was

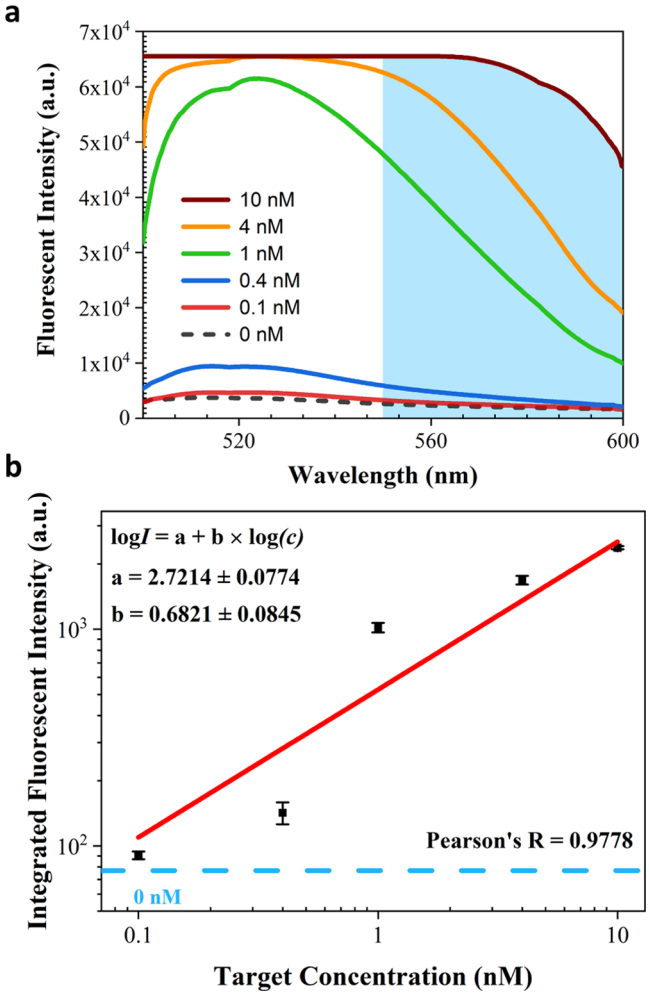

Figure 5. IMPACT chip performance with different ASFV target DNA concentrations. (a) Uncorrected emission curve of the collected supernatant with a target concentration ranging from 0.1 to 10 nM. The shaded area indicates the range used for integration to obtain data for part (b) (550–600 nm). (b) Integrated intensity of the collected supernatant versus target concentration on a logarithmic scale (Pearson's R = 0.9778). Error bars are standard deviation of the mean. Parameter "a" in the equation indicates the expected intensity value (on a log scale) for a sample with 1 nM of target DNA present. Parameter b represents the slope of the curve fit on the log–log scale, meaning for every order of magnitude increase in concentration, the expected logarithmic intensity will increase by 0.6821.

detected, demonstrating this powerful ultra-low background detection. This is an important improvement for molecular diagnostics, especially in low light settings in which the amount of background fluorescence present can significantly affect the detection limit.[36,37] Leveraging this advantage with increasing the aspect ratio either with PDMS or a silicon substrate will be able to further increase the accuracy and robustness of the device and improve the limit of detection.

The IMPACT chip offers a simple one-step detection strategy and does not require off-chip incubation. Traditional nucleic acid-based detection requires stringent multiprobe hybridization, and thus, washing is slow and complicated.[38,39] In this work, the CRISPR complex is quickly mixed with the target sample, and then, the CRISPR/crRNA/target DNA complex is injected into the channel for on-chip detection. The chip sits on a hotplate set at 37 °C and does not need thermal

https://dx.doi.org/10.1021/acsomega.0c03917
ACS Omega 2020, 5, 27433−27441

cycling with temperature control like PCR.[40,41] Thus, the detection system we developed is much simpler and more compact, ideal for POC applications.[42,43] To extend the detection limit, our system can be integrated with isothermal amplification methods such as recombinase polymerase amplification for sensitive "one-pot" target amplification and CRISPR reaction, without the background issues seen in traditional "one-pot" methods.[16,44]

An advantage of the IMPACT chip compared to other detection apparatuses such as the SHERLOCK test strip is that it is a fully enclosed microchannel without extra packaging need.[45,46] This is advantageous as the treated micropillars are sealed before molecular diagnostics. The reporter probes are immobilized within the channel, avoiding degradation issues from outside contaminants. This is particularly important when dealing with RNA target as it is susceptible to degradation by the presence of RNase.[47] Our fully integrated chip without special packaging needs is able to avoid RNase exposed in air, dust, and human hands in POC settings. In the future, PDMS-based "lifting-gate" micropumps can be integrated with the IMPACT chip core to automatically mix and transport reagents, thus completely avoiding any manual operation and contamination issues.[48,49] Furthermore, as demonstrated by our previous work, the IMPACT system can be aligned and integrated with our custom designed fluorometer to enable "sample-in" and "answer-out" viral nucleic acid detection.[21,50]

The microfabricated IMPACT chip can be used for multiplexing pathogen detection with each test that costs less than ∼10 USD (the costs per test is listed in the Supporting Information). The current design allows 30 microchannels to be patterned on a 150 mm wafer for parallel testing. For each microchannel, a unique crRNA can be designed to target a specific strain, thus enabling the screening of many strains at the same time. As PDMS chips are inexpensive and easy to fabricate, many disposable units can be produced to further improve the multiplexing capability. In addition, this design can also work with Cas13a by immobilizing ssRNA probes on the chip to directly screen RNA-based pathogen.[51,52]

This IMPACT chip concept can be extended to detect many biomarkers such as exosomes,[53] single cells,[54] and surface proteins.[55] For example, the detection sensitivity of traditional immunoassay approaches is limited due to the low binding capacity. Magnetic beads have been widely used to increase the binding affinity.[56,57] However, it is difficult to incorporate beads into the microfluidic channel as they easily settle down and get stuck in the channel. *In vivo* detection is also challenging as the beads emit strong auto-fluorescence. The micropillar arrays that we developed are patterned in the chip and can avoid those problems. In the future, on-chip treatment of blood infections can be achieved by immobilizing proper capture probes onto the IMPACT chip.[58,59]

MATERIALS AND METHODS

Device Fabrication. To create the IMPACT microfluidic chip, a mold was created using standard photolithography on a 100 mm silicon wafer. The silicon wafer was first dehydrated by baking it at 200 °C for 20 min on a hot plate. After cooling it to room temperature, SU-8 2075 (MicroChem) was spun coat onto the silicon wafer with a thickness of 120 μm. The wafer was then left to sit for 10 min on a level surface to allow for reflow and then soft baked on a hotplate at 65 °C for 10 min, followed by 20 min at 95 °C. After that, the wafer was exposed using a Karl Suss MA6 Mask Aligner for 20−25 s. It was then allowed to sit for 5 min, before receiving a post exposure bake at 80 °C for 10 min. The sample was developed for ∼10 min in SU-8 developer (MicroChem) and then sprayed down with IPA and dried. A final hard bake at 145 °C was done on a hotplate for 5 min. After the hard bake, the wafer was silanized overnight using silanization solution I (∼5% dimethyldichlorosilane in heptane) in a desiccator.

The PDMS channel was created by pouring 10:1 ratio of SYLGARD 184 Silicone Elastomer Base to SYLGARD 184 Silicone Curing Agent over the SU-8 molds and allowing it to cure. The PDMS was then peeled from the SU-8 mold, and holes (diameter of 1 mm) were punched at both ends of the channels to allow for flow of reagents through the channel. The channels were then cleaned in an ultrasonic bath for 5 min using ethanol, dried, and then cleaned again in the same manner using deionized water. The PDMS slab was then bonded to a precleaned glass substrate by treating both with oxygen plasma (Electro-Technic Products) for 2 min, followed by pressing the substrate and PDMS together. The device was immediately baked on a hotplate overnight at ∼125 °C.

Surface Modification. The device was filled with 10% APTES (Sigma-Aldrich, APTES in ethanol). A total of 75 μL of the solution was flown into the channels at a flow rate of 15 μL/min using a syringe pump (WPI, SP2201). The APTES solution was then left to incubate in the channel for 10 min and washed with 96% ethanol. After washing, the remaining liquid in the channel was drained by a syringe filled with air and then with a compressed air canister to dry the channel. The channel was then baked on a hotplate at 125 °C for 30 min. GA solution (8%) in DI water was next flown to fill the channel in the same manner, as described above, but was allowed to incubate for a full hour after the 75 μL of solution was flown through. The channel was then flushed with DI water and dried with air.

Streptavidin Immobilization. After surface treatment, each channel was injected with 20 μL of streptavidin (ThermoFisher Scientific, Streptavidin S888) at a concentration of 4 mg/ml using a 23 GA microliter syringe (Hamilton). As each channel has a volume of ∼10 μL, any excess solution was allowed to exit to the outlet. The solution was left in the channel for 2 h to incubate. The channels were then flushed with DI water and dried with air.

Surface Characterization. A goniometer system (model 260, Ramé-Hart) was used to characterize the chemically treated PDMS surface. A sessile droplet (∼4 μL) of deionized water was placed on the PDMS surface with an automated dispensing system (part no. 100-22). The static water contact angle was immediately measured by using DROPimage Matrix software, provided by Ramé-Hart.

Reporter Probe Immobilization. In a similar manner as the streptavidin was applied, 20 μL of probe solution in PBS buffer (Gibco TM, PH 7.4) was injected into the channel with a microliter syringe and allowed to incubate for 3 h, regardless of whether a photocleavable linker was attached to DNA bases.

UV Cleavage. A reporter probe with a UV cleavable linker was cleaved by using a UV light (wavelength: 311 nm). Briefly, the sample was placed under UV light with the glass side of the channel facing the light, at a distance of ∼5 cm from the UV lamp to the glass sealing the channel. The light was then turned on, and the sample was exposed to the UV light for 10 min. Finally, the released reporters were retrieved by injecting 75 μL of DI water into the channel.

https://dx.doi.org/10.1021/acsomega.0c03917
ACS Omega 2020, 5, 27433−27441

Solid-Phase CRISPR-Cas12a Detection. LbCas12a (New England BioLabs, Inc.) with a concentration of 50 nM was preassembled with 62.5 nM crRNA (IDT, Inc.) at room temperature for 10 min. Then, LbCas12a-crRNA complexes were mixed with 1× binding buffer and 14.75 μL Nuclease Free Water (IDT, Inc.) to reach a 20 μL reaction volume. After adding ASFV target DNA with various concentrations into the mixture, the detection assay was activated and immediately injected into the IMPACT chip. The device was incubated on a hotplate at 37 °C for 2 h to allow for optimized reaction. Finally, the cleaved product was retrieved from the channel and evaluated by a custom-designed fluorometer. To ensure reproducibility, each experiment was repeated three times on three independent microchannels.

Fluorescence Quantification. To quantify the fluorescence intensity of the ssDNA reporter probes, a custom-designed fluorometer was used and has been reported before.[21,50] Briefly, a continuous wave laser with an emission peak at 488 nm (Sapphire 488 LP, Coherent) was aligned under a reservoir filled with fluorescent molecules. The fluorescence signal was collected by an off-axis parabolic mirror and a fiber coupled mini USB spectrometer (USB 2000+, Ocean Optics). To reduce background noise from the excitation light, a 488 nm notch filter (Thorlabs, Inc.) was placed in front of the optical fiber.

■ ASSOCIATED CONTENT

Supporting Information

The Supporting Information is available free of charge at https://pubs.acs.org/doi/10.1021/acsomega.0c03917.

> Fluorescence images of the surface modified with APTES−GA (positive control) and APTES−valeraldehyde (negative control), negative control images of Figure 1g,h which did not receive any surface modification, and table of estimated costs for each test performed in this paper (PDF)

■ AUTHOR INFORMATION

Corresponding Author

Ke Du − *Department of Mechanical Engineering, Department of Microsystems Engineering, and School of Chemistry and Materials Science, Rochester Institute of Technology, Rochester, New York 14623, United States;* orcid.org/0000-0002-6837-0927; Email: ke.du@rit.edu

Authors

Kenneth N. Hass − *Department of Mechanical Engineering, Rochester Institute of Technology, Rochester, New York 14623, United States*

Mengdi Bao − *Department of Mechanical Engineering, Rochester Institute of Technology, Rochester, New York 14623, United States*

Qian He − *Center of Precision Medicine and Healthcare, Tsinghua-Berkeley Shenzhen Institute, Shenzhen, Guangdong Province 518055, China*

Li Liu − *Department of Microsystems Engineering, Rochester Institute of Technology, Rochester, New York 14623, United States*

Jiacheng He − *Department of Mechanical Engineering, Rochester Institute of Technology, Rochester, New York 14623, United States*

Myeongkee Park − *Department of Chemistry, Dong-A University, Busan 49315, Republic of Korea;* orcid.org/0000-0002-5307-2564

Peiwu Qin − *Center of Precision Medicine and Healthcare, Tsinghua-Berkeley Shenzhen Institute, Shenzhen, Guangdong Province 518055, China;* orcid.org/0000-0002-7829-8973

Complete contact information is available at: https://pubs.acs.org/10.1021/acsomega.0c03917

Author Contributions

K.N.H. and M.B. contributed equally. The manuscript was written through contributions of all authors. K.N.H., M.B., and K.D. designed the experiments. K.N.H., M.B., Q.H., L.L., and J.H. conducted the experiments. K.N.H., M.B., and K.D. wrote the manuscript. All the authors commented on the manuscript.

Funding

This project was supported by the Burroughs Wellcome Fund (BWF) 2019 Collaborative Research Travel Grant (1019955), RIT seed fund, and RIT Start-Up fund.

Notes

The authors declare no competing financial interest.

■ ACKNOWLEDGMENTS

This research used resources of the Center for Functional Nanomaterials, which is a U.S. DOE Office of Science Facility, at Brookhaven National Laboratory under contract no. DE-SC0012704. The authors would like to thank Wenrong He and Personalize Healthcare Technology (PHT180) at the RIT for schematic design.

■ ABBREVIATIONS

IMPACT, Integrated Micropillar Polydimethylsiloxane Accurate CRISPR Detection; ASFV, African swine fever virus; POC, point-of-care; LOC, lab-on-chip; PCR, polymerase chain reaction; CRISPR, clustered regularly interspaced short palindromic repeats; ssDNA, single-stranded DNA; PDMS, polydimethylsiloxane; APTES, (3-aminopropyl)triethoxysilane

■ REFERENCES

(1) Coronavirus Update (Live): 18,802,282 Cases and 706,443 Deaths from COVID-19 Virus Pandemic - Worldometer, https://www.worldometers.info/coronavirus/ (accessed Aug 5, 2020).

(2) COVID-19 Map. https://coronavirus.jhu.edu/map.html (accessed Aug 5, 2020).

(3) Cubillos, C.; Gómez-Sebastian, S.; Moreno, N.; Nuñez, M. C.; Mulumba-Mfumu, L. K.; Quembo, C. J.; Heath, L.; Etter, E. M. C.; Jori, F.; Escribano, J. M.; Blanco, E. African Swine Fever Virus Serodiagnosis: A General Review with a Focus on the Analyses of African Serum Samples. *Virus Res.* **2013**, *173*, 159−167.

(4) Srikrishna, D.; Dhillon, R. S.; Beier, D. We Need a Cheap Way to Diagnose Coronavirus. *Harv. Bus. Rev.*, **2020**.

(5) Borca, M. V.; Ramirez-Medina, E.; Silva, E.; Vuono, E.; Rai, A.; Pruitt, S.; Holinka, L. G.; Velazquez-Salinas, L.; Zhu, J.; Gladue, D. P. Development of a Highly Effective African Swine Fever Virus Vaccine by Deletion of the I177L Gene Results in Sterile Immunity against the Current Epidemic Eurasia Strain. *J. Virol.* **2020**, *94*, No. e02017.

(6) Chen, W.; Zhao, D.; He, X.; Liu, R.; Wang, Z.; Zhang, X.; Li, F.; Shan, D.; Chen, H.; Zhang, J.; Wang, L.; Wen, Z.; Wang, X.; Guan, Y.; Liu, J.; Bu, Z. A Seven-Gene-Deleted African Swine Fever Virus Is Safe and Effective as a Live Attenuated Vaccine in Pigs. *Sci. China Life Sci.* **2020**, *63*, 623.

(7) Pang, J.; Wang, M. X.; Ang, I. Y. H.; Tan, S. H. X.; Lewis, R. F.; Chen, J. I.-P.; Gutierrez, R. A.; Gwee, S. X. W.; Chua, P. E. Y.; Yang, Q.; Ng, X. Y.; Yap, R. K. S.; Tan, H. Y.; Teo, Y. Y.; Tan, C. C.; Cook,

A. R.; Yap, J. C.-H.; Hsu, L. Y. Potential Rapid Diagnostics, Vaccine and Therapeutics for 2019 Novel Coronavirus (2019-NCoV): A Systematic Review. *J. Clin. Med.* **2020**, *9*, 623.
(8) Otter, J. A.; Donskey, C.; Yezli, S.; Douthwaite, S.; Goldenberg, S. D.; Weber, D. J. Transmission of SARS and MERS Coronaviruses and Influenza Virus in Healthcare Settings: The Possible Role of Dry Surface Contamination. *J. Hosp. Infect.* **2016**, *92*, 235−250.
(9) Pai, N. P.; Vadnais, C.; Denkinger, C.; Engel, N.; Pai, M. Point-of-Care Testing for Infectious Diseases: Diversity, Complexity, and Barriers in Low- And Middle-Income Countries. *PLoS Med.* **2012**, *9*, No. e1001306.
(10) Xiao, S.-Y.; Wu, Y.; Liu, H. Evolving Status of the 2019 Novel Coronavirus Infection: Proposal of Conventional Serologic Assays for Disease Diagnosis and Infection Monitoring. *J. Med. Virol.* **2020**, *92*, 464.
(11) Zhu, H.; Fohlerová, Z.; Pekárek, J.; Basova, E.; Neužil, P. Recent Advances in Lab-on-a-Chip Technologies for Viral Diagnosis. *Biosens. Bioelectron.* **2020**, *153*, 112041.
(12) Wang, A.; Jia, R.; Liu, Y.; Zhou, J.; Qi, Y.; Chen, Y.; Liu, D.; Zhao, J.; Shi, H.; Zhang, J.; Zhang, G. Development of a Novel Quantitative Real-Time PCR Assay with Lyophilized Powder Reagent to Detect African Swine Fever Virus in Blood Samples of Domestic Pigs in China. *Transboundary Emerging Dis.* **2020**, *67*, 284−297.
(13) Fernández-Carballo, B. L.; McBeth, C.; McGuiness, I.; Kalashnikov, M.; Baum, C.; Borrós, S.; Sharon, A.; Sauer-Budge, A. F. Continuous-Flow, Microfluidic, QRT-PCR System for RNA Virus Detection. *Anal. Bioanal. Chem.* **2018**, *410*, 33−43.
(14) Cohen, J.; Kupferschmidt, K. Labs Scramble to Produce New Coronavirus Diagnostics. *Science* **2020**, *367*, 727.
(15) Hao, W.; Li, M. Clinical Features of Atypical 2019 Novel Coronavirus Pneumonia with an Initially Negative RT-PCR Assay. *J. Infect.* **2020**, *80*, 671.
(16) Chen, J. S.; Ma, E.; Harrington, L. B.; Da Costa, M.; Tian, X.; Palefsky, J. M.; Doudna, J. A. CRISPR-Cas12a Target Binding Unleashes Indiscriminate Single-Stranded DNase Activity. *Science* **2018**, *360*, 436−439.
(17) Kim, D.; Kim, J.; Hur, J. K.; Been, K. W.; Yoon, S.-h.; Kim, J.-S. Genome-Wide Analysis Reveals Specificities of Cpf1 Endonucleases in Human Cells. *Nat. Biotechnol.* **2016**, *34*, 863−868.
(18) Vijayaraghavan, R.; Izgorodin, A.; Ganesh, V.; Surianarayanan, M.; MacFarlane, D. R. Long-Term Structural and Chemical Stability of DNA in Hydrated Ionic Liquids. *Angew. Chem., Int. Ed.* **2010**, *49*, 1631−1633.
(19) Tsougeni, K.; Tserepi, A.; Constantoudis, V.; Gogolides, E.; Petrou, P. S.; Kakabakos, S. E. Plasma Nanotextured PMMA Surfaces for Protein Arrays: Increased Protein Binding and Enhanced Detection Sensitivity. *Langmuir* **2010**, *26*, 13883−13891.
(20) Yu, X.; Xia, Y.; Tang, Y.; Zhang, W.-L.; Yeh, Y.-T.; Lu, H.; Zheng, S.-Y. A Nanostructured Microfluidic Immunoassay Platform for Highly Sensitive Infectious Pathogen Detection. *Small* **2017**, *13*, 1700425.
(21) He, Q.; Yu, D.; Bao, M.; Korensky, G.; Chen, J.; Shin, M.; Kim, J.; Park, M.; Qin, P.; Du, K. High-Throughput and All-Solution Phase African Swine Fever Virus (ASFV) Detection Using CRISPR-Cas12a and Fluorescence Based Point-of-Care System. *Biosens. Bioelectron.* **2020**, *154*, 112068.
(22) Bao, M.; Jensen, E. C.; Chang, Y.; Korensky, G.; Du, K. Magnetic Bead-Quantum Dot (MB-Qdot) CRISPR Assay for Simple Viral DNA Detection. *ACS Appl. Mater. Interfaces* **2020**, *12* (39), 43435−43443.
(23) Broughton, J. P.; Deng, X.; Yu, G.; Fasching, C. L.; Servellita, V.; Singh, J.; Miao, X.; Streithorst, J. A.; Granados, A.; Sotomayor-Gonzalez, A.; Zorn, K.; Gopez, A.; Hsu, E.; Gu, W.; Miller, S.; Pan, C.-Y.; Guevara, H.; Wadford, D. A.; Chen, J. S.; Chiu, C. Y. CRISPR−Cas12-Based Detection of SARS-CoV-2. *Nat. Biotechnol.* **2020**, *38*, 870−874.
(24) Bruch, R.; Baaske, J.; Chatelle, C.; Meirich, M.; Madlener, S.; Weber, W.; Dincer, C.; Urban, G. A. CRISPR/Cas13a-Powered Electrochemical Microfluidic Biosensor for Nucleic Acid Amplification-Free MiRNA Diagnostics. *Adv. Mater.* **2019**, *31*, 1970365.
(25) Mani, N. K.; Rudiuk, S.; Baigl, D. Spatially Controlled DNA Unzipping by Microfluidic Interface Positioning on a Molecule Perpendicular to a Multicomponent Flow. *Chem. Commun.* **2013**, *49*, 6858−6860.
(26) Liu, W.; Samanta, S. K.; Smith, B. D.; Isaacs, L. Synthetic Mimics of Biotin/(Strept)Avidin. *Chem. Soc. Rev.* **2017**, *46*, 2391.
(27) Lee, K.; Choi, S.; Yang, C.; Wu, H.-C.; Yu, J. Autofluorescence Generation and Elimination: A Lesson from Glutaraldehyde. *Chem. Commun.* **2013**, *49*, 3028−3030.
(28) Kamar, R. I.; Banigan, E. J.; Erbas, A.; Giuntoli, R. D.; Olvera de la Cruz, M.; Johnson, R. C.; Marko, J. F. Facilitated Dissociation of Transcription Factors from Single DNA Binding Sites. *Proc. Natl. Acad. Sci. U.S.A.* **2017**, *114*, E3251−E3257.
(29) Xu, S.; Zhan, J.; Man, B.; Jiang, S.; Yue, W.; Gao, S.; Guo, C.; Liu, H.; Li, Z.; Wang, J.; Zhou, Y. Real-Time Reliable Determination of Binding Kinetics of DNA Hybridization Using a Multi-Channel Graphene Biosensor. *Nat. Commun.* **2017**, *8*, 14902.
(30) Qian, L.; Wang, J.; Yang, Z.; Yan, G. Fabrication of Ultra-Deep High-Aspect-Ratio Isolation Trench without Void and Its Application. *2010 IEEE 5th International Conference on Nano/Micro Engineered and Molecular Systems*, 2010; pp 654−657.
(31) Vijselaar, W.; Westerik, P.; Veerbeek, J.; Tiggelaar, R. M.; Berenschot, E.; Tas, N. R.; Gardeniers, H.; Huskens, J. Spatial Decoupling of Light Absorption and Catalytic Activity of Ni−Mo-Loaded High-Aspect-Ratio Silicon Microwire Photocathodes. *Nat. Energy* **2018**, *3*, 185−192.
(32) Li, X.; Yang, Y.; Liu, L.; Chen, Y.; Chu, M.; Sun, H.; Shan, W.; Chen, Y. 3D-Printed Cactus-Inspired Spine Structures for Highly Efficient Water Collection. *Adv. Mater. Interfaces* **2020**, *7*, 1901752.
(33) Liu, X.; Gu, H.; Wang, M.; Du, X.; Gao, B.; Elbaz, A.; Sun, L.; Liao, J.; Xiao, P.; Gu, Z. 3D Printing of Bioinspired Liquid Superrepellent Structures. *Adv. Mater.* **2018**, *30*, 1800103.
(34) Su, Y.; Hammond, M. C. RNA-Based Fluorescent Biosensors for Live Cell Imaging of Small Molecules and RNAs. *Curr. Opin. Biotechnol.* **2020**, *63*, 157−166.
(35) Tsou, J.-H.; Leng, Q.; Jiang, F. A CRISPR Test for Rapidly and Sensitively Detecting Circulating EGFR Mutations. *Diagnostics* **2020**, *10*, 114.
(36) Gao, P.; Prunsche, B.; Zhou, L.; Nienhaus, K.; Nienhaus, G. U. Background Suppression in Fluorescence Nanoscopy with Stimulated Emission Double Depletion. *Nat. Photon.* **2017**, *11*, 163−169.
(37) Zhao, M.; Nicovich, P. R.; Janco, M.; Deng, Q.; Yang, Z.; Ma, Y.; Böcking, T.; Gaus, K.; Gooding, J. J. Ultralow- and Low-Background Surfaces for Single-Molecule Localization Microscopy of Multistep Biointerfaces for Single-Molecule Sensing. *Langmuir* **2018**, *34*, 10012−10018.
(38) Liu, S.; Fang, L.; Wang, Y.; Wang, L. Universal Dynamic DNA Assembly-Programmed Surface Hybridization Effect for Single-Step, Reusable, and Amplified Electrochemical Nucleic Acid Biosensing. *Anal. Chem.* **2017**, *89*, 3108−3115.
(39) Zhang, J.; Wang, L.-L.; Hou, M.-F.; Xia, Y.-K.; He, W.-H.; Yan, A.; Weng, Y.-P.; Zeng, L.-P.; Chen, J.-H. A Ratiometric Electrochemical Biosensor for the Exosomal MicroRNAs Detection Based on Bipedal DNA Walkers Propelled by Locked Nucleic Acid Modified Toehold Mediate Strand Displacement Reaction. *Biosens. Bioelectron.* **2018**, *102*, 33−40.
(40) Lee, S. H.; Yu, J.; Hwang, G.-H.; Kim, S.; Kim, H. S.; Ye, S.; Kim, K.; Park, J.; Park, D. Y.; Cho, Y.-K.; Kim, J.-S.; Bae, S. CUT-PCR: CRISPR-Mediated, Ultrasensitive Detection of Target DNA Using PCR. *Oncogene* **2017**, *36*, 6823−6829.
(41) Zhang, M.; Liu, C.; Shi, Y.; Wu, J.; Wu, J.; Chen, H. Selective Endpoint Visualized Detection of Vibrio Parahaemolyticus with CRISPR/Cas12a Assisted PCR Using Thermal Cycler for on-Site Application. *Talanta* **2020**, *214*, 120818.
(42) Foudeh, A. M.; Fatanat Didar, T.; Veres, T.; Tabrizian, M. Microfluidic Designs and Techniques Using Lab-on-a-Chip Devices

https://dx.doi.org/10.1021/acsomega.0c03917
ACS Omega 2020, 5, 27433−27441

for Pathogen Detection for Point-of-Care Diagnostics. *Lab Chip* **2012**, *12*, 3249−3266.
(43) Nasseri, B.; Soleimani, N.; Rabiee, N.; Kalbasi, A.; Karimi, M.; Hamblin, M. R. Point-of-Care Microfluidic Devices for Pathogen Detection. *Biosens. Bioelectron.* **2018**, *117*, 112−128.
(44) Wang, B.; Wang, R.; Wang, D.; Wu, J.; Li, J.; Wang, J.; Liu, H.; Wang, Y. Cas12aVDet: A CRISPR/Cas12a-Based Platform for Rapid and Visual Nucleic Acid Detection. *Anal. Chem.* **2019**, *91*, 12156−12161.
(45) Kellner, M. J.; Koob, J. G.; Gootenberg, J. S.; Abudayyeh, O. O.; Zhang, F. SHERLOCK: Nucleic Acid Detection with CRISPR Nucleases. *Nat. Protoc.* **2019**, *14*, 2986−3012.
(46) Tsou, J.-H.; Leng, Q.; Jiang, F. A CRISPR Test for Detection of Circulating Nuclei Acids. *Transl. Oncol.* **2019**, *12*, 1566−1573.
(47) Living with RNase - US. https://www.thermofisher.com/us/en/home/references/ambion-tech-support/nuclease-enzymes/general-articles/ten-sources-of-rnase-contamination.html (accessed Feb 29, 2020).
(48) Du, K.; Cai, H.; Park, M.; Wall, T. A.; Stott, M. A.; Alfson, K. J.; Griffiths, A.; Carrion, R.; Patterson, J. L.; Hawkins, A. R.; Schmidt, H.; Mathies, R. A. Multiplexed Efficient On-Chip Sample Preparation and Sensitive Amplification-Free Detection of Ebola Virus. *Biosens. Bioelectron.* **2017**, *91*, 489−496.
(49) Du, K.; Park, M.; Griffiths, A.; Carrion, R.; Patterson, J.; Schmidt, H.; Mathies, R. Microfluidic System for Detection of Viral RNA in Blood Using a Barcode Fluorescence Reporter and a Photocleavable Capture Probe. *Anal. Chem.* **2017**, *89*, 12433−12440.
(50) Qin, P.; Park, M.; Alfson, K. J.; Tamhankar, M.; Carrion, R.; Patterson, J. L.; Griffiths, A.; He, Q.; Yildiz, A.; Mathies, R.; Du, K. Rapid and Fully Microfluidic Ebola Virus Detection with CRISPR-Cas13a. *ACS Sens.* **2019**, *4*, 1048−1054.
(51) Bruch, R.; Urban, G. A.; Dincer, C. CRISPR/Cas Powered Multiplexed Biosensing. *Trends Biotechnol.* **2019**, *37*, 791−792.
(52) Li, Y.; Li, S.; Wang, J.; Liu, G. CRISPR/Cas Systems towards Next-Generation Biosensing. *Trends Biotechnol.* **2019**, *37*, 730−743.
(53) Zhang, P.; He, M.; Zeng, Y. Ultrasensitive Microfluidic Analysis of Circulating Exosomes Using a Nanostructured Graphene Oxide/Polydopamine Coating. *Lab Chip* **2016**, *16*, 3033−3042.
(54) Song, Y.; Tian, T.; Shi, Y.; Liu, W.; Zou, Y.; Khajvand, T.; Wang, S.; Zhu, Z.; Yang, C. Enrichment and Single-Cell Analysis of Circulating Tumor Cells. *Chem. Sci.* **2017**, *8*, 1736−1751.
(55) Aoyama, S.; Monden, K.; Akiyama, Y.; Yamada, M.; Seki, M. Enhanced Immunoadsorption on Imprinted Polymeric Microstructures with Nanoengineered Surface Topography for Lateral Flow Immunoassay Systems. *Anal. Chem.* **2019**, *91*, 13377−13382.
(56) Jalal, U. M.; Jin, G. J.; Eom, K. S.; Kim, M. H.; Shim, J. S. On-Chip Signal Amplification of Magnetic Bead-Based Immunoassay by Aviating Magnetic Bead Chains. *Bioelectrochemistry* **2018**, *122*, 221−226.
(57) Roth, S.; Hadass, O.; Cohen, M.; Verbarg, J.; Wilsey, J.; Danielli, A. Photobleaching: Improving the Sensitivity of Fluorescence-Based Immunoassays by Photobleaching the Autofluorescence of Magnetic Beads (Small 3/2019). *Small* **2019**, *15*, 1970016.
(58) Didar, T. F.; Cartwright, M. J.; Rottman, M.; Graveline, A. R.; Gamini, N.; Watters, A. L.; Leslie, D. C.; Mammoto, T.; Rodas, M. J.; Kang, J. H.; Waterhouse, A.; Seiler, B. T.; Lombardo, P.; Qendro, E. I.; Super, M.; Ingber, D. E. Improved Treatment of Systemic Blood Infections Using Antibiotics with Extracorporeal Opsonin Hemoadsorption. *Biomaterials* **2015**, *67*, 382−392.
(59) Kim, G.; Vinerean, H.; Gaitas, A. A Novel Pathogen Capturing Device for Removal and Detection. *Sci. Rep.* **2017**, *7*, 5552.

https://dx.doi.org/10.1021/acsomega.0c03917
ACS Omega 2020, 5, 27433−27441